Hadronic ^{3}Heη production near threshold

H.-H. Adam,* I. Geck, A. Khoukaz, T. Lister,† R. Santo, S. Steltenkamp,‡ and A. Täschner
Institut für Kernphysik, Universität Münster, Wilhelm-Klemm-Str. 9, Münster, D-48149, Germany

E. Czerwiński, R. Czyżykiewicz, M. Janusz, L. Jarczyk, B. Kamys, P. Klaja, P. Moskal, C. Piskor-Ignatowicz, J. Przerwa, and J. Smyrski
Nuclear Physics Department, Jagellonian University, Cracow, PL-30-059, Poland

D. Grzonka, K. Kilian, W. Oelert, T. Sefzick, P. Winter, M. Wolke, and P. Wüstner
IKP and ZEL Forschungszentrum Jülich, Jülich, D-52425, Germany

A. Budzanowski
Institute of Nuclear Physics, Cracow, PL-31-342, Poland

T. Rożek, M. Siemaszko, and W. Zipper
Institute of Physics, University of Silesia, Katowice, PL-40-007, Poland

(Received 13 February 2006; revised manuscript received 15 September 2006; published 18 January 2007)

Measurements of η meson production in proton-deuteron collisions have been performed using the COSY-11 facility at COSY (Jülich). Results on total and differential cross sections for the $pd \to {}^3\mathrm{He}\eta$ reaction are presented at five excess energies between $Q = 5.0$ and $Q = 40.6$ MeV. The angular distributions show a transition from an almost isotropic emission close to threshold to a highly anisotropic distribution at higher excess energies. The total cross sections reveal a strong η-^{3}He final state interaction, corresponding to a scattering length of $|\Re(a)| = (4.2 \pm 0.5)$ fm and $\Im(a) = (0.4 \pm 1.9)$ fm.

DOI: 10.1103/PhysRevC.75.014004 PACS number(s): 25.40.Ve, 13.60.Le, 13.75.−n, 14.40.Aq

I. INTRODUCTION

Within the field of particle interactions, the formation of bound or quasibound states between an η meson and a nucleon or nucleus, creating so-called η-mesic nuclei, has attracted a lot of both theoretical and experimental interest. Predicted by Haider and Liu [1], the interaction of the η with a nucleus is expected to be attractive, as in the elementary η-N interaction [2–4], and therefore allows for the formation of a bound state. Recently, it was argued that the η bound state will deliver information about the singlet component of the η meson [5]. Although the strength of the attractive potential is supposed to increase with the mass of the nucleus, the answer to the question as to which is the lightest η-mesic nucleus is still unknown.

Therefore, close-to-threshold data on the $pd \to {}^3\mathrm{He}\eta$ reaction are of great interest for studying the strong η-nucleus final state interaction at low energies, which may provide a signal for the existence of quasibound η-nucleus states [6]. As observed close to threshold at the SPES-IV and SPES-II spectrometers at the SATURNE laboratory [7,8], the η-production cross section in the $pd \to {}^3\mathrm{He}\eta$ reaction reveals remarkable features. In addition to the unexpectedly large cross section for this channel as compared to, e.g., $pd \to {}^3\mathrm{He}\pi^0$, the excitation function has a maximum very close to the production threshold and a significant drop of the production amplitude with increasing energy within only a few MeV, which is in complete contrast to expectations based upon phase space. Furthermore, the center-of-mass angular distributions of the η mesons emitted near threshold were reported to be consistent with s-wave production and to exhibit no major contributions from higher partial waves. This behavior differs from the corresponding data on the π^0-production cross section, where a strong p-wave contribution is present even very close to threshold [9].

In order to describe this near-threshold behavior, a classical two-step mechanism was proposed by Kilian and Nann [10]. However, quantum mechanical calculations by Fäldt and Wilkin [11] within this model only succeeded in reproducing the square of the production amplitude at threshold to within a factor of 2.4. Moreover, to describe the observed rapid drop of the production amplitude with increasing energy, the two-step approach had to include a strong η-^{3}He final state interaction (FSI) with a large η-^{3}He scattering length.

Further measurements, performed at a higher excess energy of ∼50 MeV by the COSY-GEM Collaboration [12], yielded a highly nonisotropic angular distribution. The description using the refined two-step model prediction [12], adjusted to fit to the data at energies very close to threshold, significantly underestimates the value of the total cross section. Therefore, a different reaction mechanism, based on the excitation of the $N^*(1535)$ resonance, has been suggested. However, this model

*Electronic address: adamh@uni-muenster.de; present address: IVV Naturwissenschaften, Universität Münster, Institut für Festkörpertheorie, Wilhelm-Klemm-Str. 10, Münster, D-48149, Germany.
†Present address: Robert-Janker-Klinik, Villenstr. 4, Bonn, D-53129, Germany.
‡Present address: Institut für Physikalische Chemie, Universität Mainz, Jakob-Welder-Weg 11-15, Mainz, D-55128, Germany.

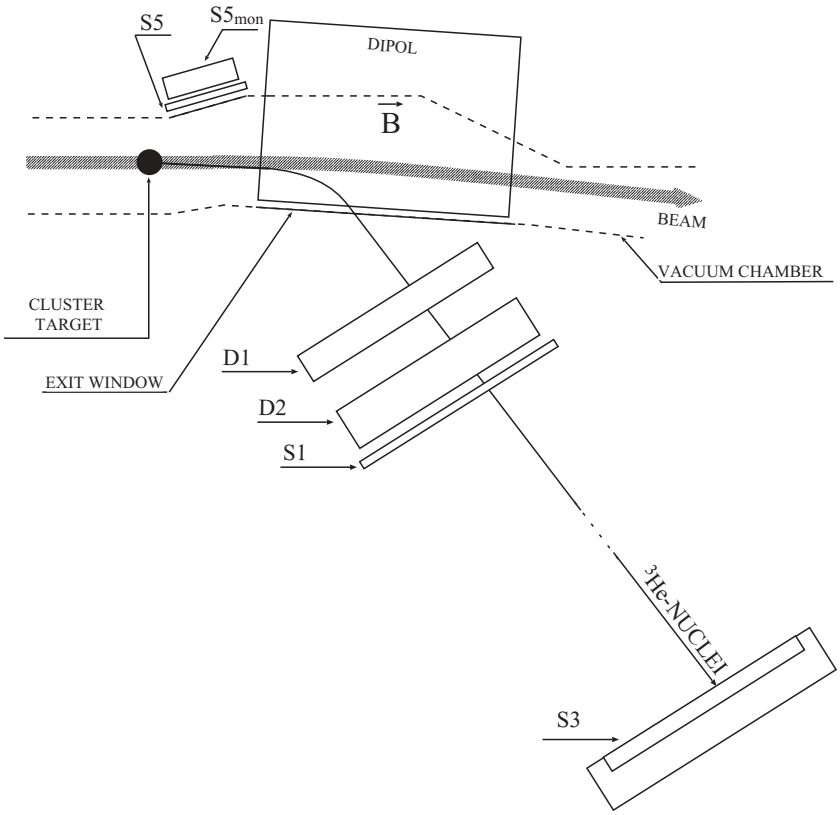

FIG. 1. Sketch of COSY-11 installation. The magnetic spectrometer, consisting of drift chambers and scintillation and silicon-pad detectors is located in an arc region of the cooler synchrotron COSY at the Forschungszentrum Jülich.

prediction, scaled to fit the COSY-GEM data point, fails to reproduce the observed shape of the previously determined excitation function in the near-threshold region.

Additional studies have also been carried out by the WASA/PROMICE Collaboration at η excess energies between $\sim$22 and $\sim$120 MeV [13], yielding anisotropic angular distributions for all the measurements, in agreement with the GEM results, but with total cross sections that can be described by neither the η-^{3}He FSI nor the predicted shape of the resonance model excitation function.

Therefore, to investigate both the shape of the excitation function, as well as the development of the angular distributions with increasing excess energy, additional measurements on the $pd \rightarrow {}^3\mathrm{He}X$ reaction have been carried out at η excess energies in the range of $Q = 5.0$ to 40.6 MeV using the COSY-11 installation.

II. EXPERIMENT

The COSY-11 installation is an internal experimental facility located in an arc section of the cooler synchrotron (COSY) [14] at the Forschungszentrum Jülich. For details, see Ref. [15–17].

A cluster-jet target [18], operated with deuterium gas, was used to provide a dense deuteron target for the stochastically cooled, high-precision proton beam of COSY. The COSY-11 facility makes use of one of the accelerator dipoles as a spectrometer magnet to separate the positively charged reaction ejectiles (e.g., ^{3}He nuclei) from the circulating beam and guide them toward the forward detection system (Fig. 1). This system consists of a set of two drift chambers (D1, D2), used for track reconstruction, and two large scintillator hodoscopes (S1, S3). Tracing back the tracks through the magnetic field of the spectrometer magnet [19–21] to the fixed interaction point leads to a momentum reconstruction with a precision of better than 1% [4]. The scintillation detectors S1 (placed directly behind the second drift chamber) and S3 (placed a distance farther of roughly 9 m) are used as a start and stop combination for time-of-flight measurements. Particle identification can thus be performed by reconstructing the mass of the ejectiles using the momentum and velocity information, yielding a full four-momentum vector reconstruction for all detected positively charged particles.

To obtain cross sections, the $pd \rightarrow {}^3\mathrm{He}X$ data are normalized using the results on the proton-deuteron elastic scattering that was measured in parallel. For this purpose, additional silicon-pad and scintillation detectors (S5 and $\mathrm{S5_{mon}}$) in the target region are used to detect the elastically scattered deuteron in coincidence with the detected proton in the forward-detection system (D1&2, S1) [16,22]. The complementary case of a deuteron in the forward direction and a coincident proton in the monitor detector is allowed by kinematics. However, it is not observed in the experiment because of the large momentum transfers in this case, which make deuteron breakup highly probable.

III. DATA ANALYSIS

The reaction channel $pd \rightarrow {}^3\mathrm{He}\eta$ was studied by detecting the emitted ^{3}He nuclei and identifying the η mesons through

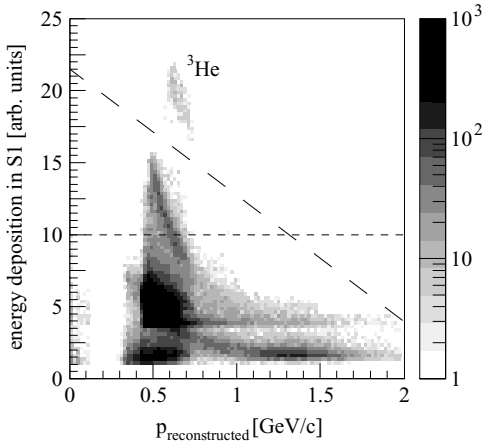

FIG. 2. ^{3}He selection from events triggered by the detection system for a beam momentum of 1.593 GeV/c ($Q = 10.8$ MeV). Because of the high-energy deposition of the ^{3}He nuclei in the scintillator detector S1, ^{3}He events can be separated easily from the background consisting of pions, protons, deuterons, and tritons. The dashed lines indicate the cuts on energy loss and the correlation of energy loss to the reconstructed momentum used to select the ^{3}He events.

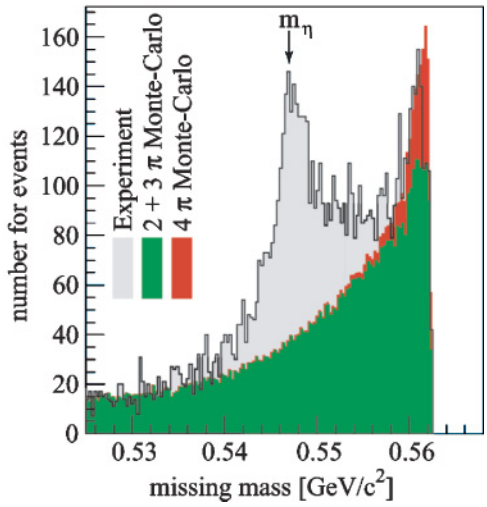

FIG. 3. (Color online) Missing-mass distribution obtained for ^{3}He events, recorded at an excess energy of 15.1 MeV. On top of the background, a peak in the range of the η mass ($m_\eta = 0.5473\,\mathrm{GeV}/c^2$) is quite prominent. By combining Monte Carlo events from reactions of the type $pd \to {}^{3}\mathrm{He}n \cdot \pi(n \geqslant 2)$ the background observed in the experiment can be described very well. The simulation was fit in magnitude to the experimental data in the region outside the η signal; for details see text.

the missing-mass technique. To separate ^{3}He events from a background of pions, protons, deuterons, and tritons, the $\Delta E/p$ information was exploited. This leads to a clear ^{3}He signal [23] due to its high-energy deposition in scintillating material [24] (Fig. 2). This positive identification allows one to determine the four-momentum vectors $P_{^3\mathrm{He}} = (\sqrt{p^2_{^3\mathrm{He}} + m^2_{^3\mathrm{He}}}, \vec{p}_{^3\mathrm{He}})$, where $\vec{p}_{^3\mathrm{He}}$ is measured with a precision of better than 1% [4].

The missing-mass plot of the $pd \to {}^{3}\mathrm{He}X$ reaction calculated for the selected ^{3}He events exhibits a clearly visible peak at the mass of the η meson on top of a background originating from multipion production (Fig. 3). This background can be reproduced well by phase-space Monte Carlo simulations of the $pd \to {}^{3}\mathrm{He}n \cdot \pi(n \geqslant 2)$ reaction channels at the corresponding beam energies. The simulations, based on the GEANT 3.21 code [25], have been carried out separately for the several charged and uncharged multipion channels. Neither the charge of the produced pions nor the two- and three-pion production processes can be distinguished in the shape of the missing-mass distribution in our limited range. This is because of the large excess energy for multipion production at the η threshold, where the shape is dominated by the acceptance of the detection system. In the case of the $pp \to pp\eta$ channel, this effect was discussed in Ref. [26].

By subtracting the scaled Monte Carlo generated multipion data from the experimental distribution, a clean missing-mass peak remains with a width of less than 6 MeV (full width at half maximum) which is in very good agreement with expectations from Monte Carlo simulations of the $pd \to {}^{3}\mathrm{He}\eta$ channel (Fig. 4). As presented in Fig. 3, the combined two- and three-pion production Monte Carlo simulations were scaled to describe the leading tail of the data, whereas the four-pion Monte Carlo simulation was scaled to describe the data at the kinematic limit.

To evaluate differential cross sections, the missing-mass technique was used for each angular bin, and the number of detected η mesons was obtained separately by subtracting the background, as for the total spectrum of Fig. 3. The ambiguity in the scaling factors for the background subtraction is reflected in the systematic error of the number of extracted η events.

To calculate the total cross section σ_{tot} from the number of η events in the missing-mass spectrum, the acceptance of the detection system and the integrated luminosity have to be known. The acceptance was determined by Monte Carlo studies. The integrated luminosity for each of the five measurements was deduced from the analysis of proton-deuteron elastic scattering. Momentum transfer distributions of $pd \to pd$ events were obtained from the angle of the recoil protons and compared with data from the literature [27–30] to obtain differential cross section information. The procedure is described in detail in Ref. [22], and the results are listed in Table I. The systematic errors arise principally from the uncertainty in the identification of elastic scattering events and the determination of the corresponding differential cross

TABLE I. Integrated luminosity determined from proton-deuteron elastic scattering.

Beam momentum (GeV/c)	Integrated luminosity		
	(nb^{-1})	σ_{stat}	σ_{syst}
1.581	51.6	±1.9%	±8.9%
1.593	62.6	±1.4%	±8.9%
1.602	62.4	±1.6%	±8.9%
1.612	66.4	±1.4%	±8.9%
1.655	73.0	±1.5%	±8.9%

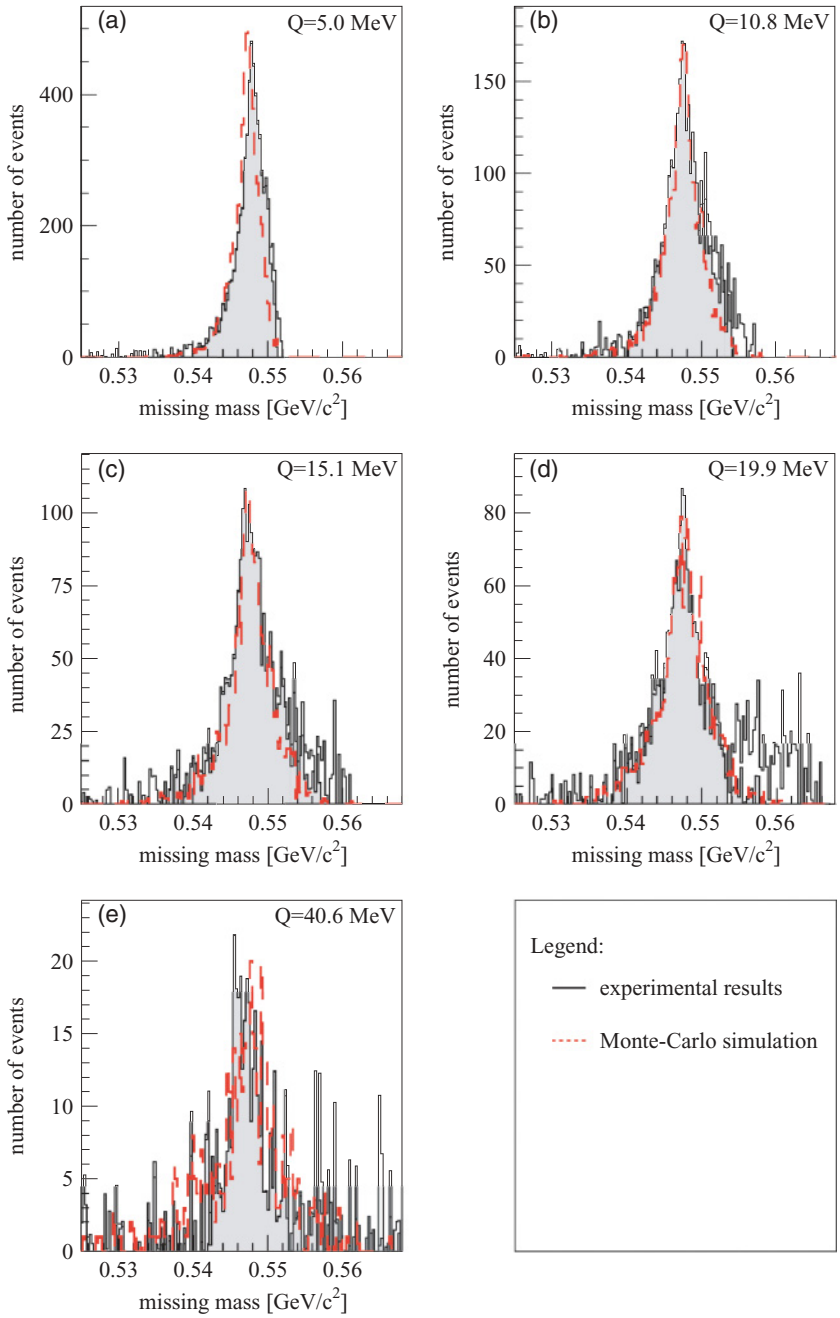

FIG. 4. (Color online) Missing-mass distribution for the $pd \rightarrow {}^3\mathrm{He}\eta$ reaction at different excess energies. The spectra have been obtained by summing up the background-subtracted missing-mass spectra in the different angular bins in the differential cross section analysis. Only the shaded parts of the peaks have been included for the determination of the cross sections. The dashed lines indicate the expectation from Monte Carlo simulations for the respective beam momenta.

section at the measured beam momenta by interpolating the published data.

IV. RESULTS

Based on the missing-mass analysis, $pd \rightarrow {}^3\mathrm{He}\eta$ differential cross sections have been extracted for all measured excess energies, with the results displayed in Fig. 5. In view of the extreme forward-folding of the ^{3}He angular distribution, the bin width in the backward hemisphere was limited by the accuracy of the center-of-mass angle reconstruction. In the forward hemisphere, the statistics allowed only one bin. However, the SPES data resulted in an angular distribution compatible with pure s-wave emission, and also the WASA/PROMICE studies presented slowly varying angular distributions for the lower excess energies. Hence, we concentrated on taking data at several excess energies, with limited statistics, rather than aiming at the extraction of high statistics angular distributions. Nevertheless, the angular distributions obtained are sufficient to extract total cross sections.

Over the range of excess energies investigated, a transition is seen from a rather flat angular distribution at the two lowest energies, as observed in Ref. [8], to a highly anisotropic behavior for the highest measured excess energy of 40.6 MeV, as in Refs. [12,13]. Therefore, it is plausible to assume pure s-wave production from threshold up to excess energies somewhere between 11 and 15 MeV. This behavior differs from that of the $pd \rightarrow {}^3\mathrm{He}\pi^0$ reaction where, already

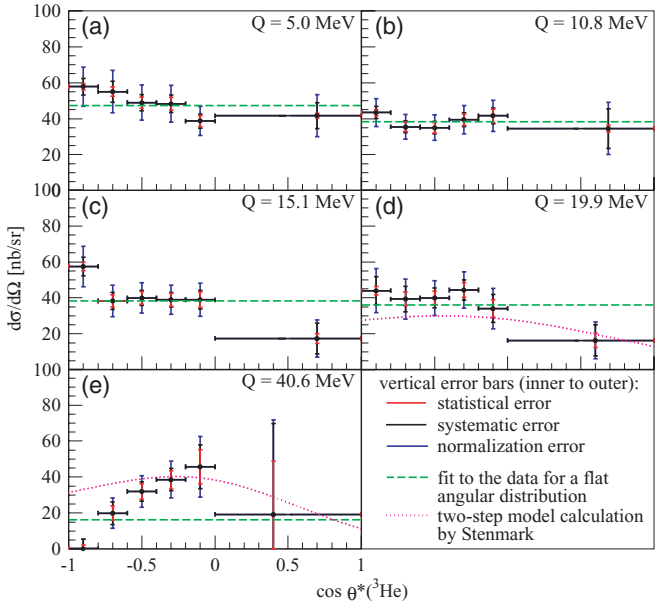

FIG. 5. (Color online) Differential cross sections determined at five different excess energies. The angular distributions of the produced ^{3}He nuclei in the center-of-mass system show a transition from a rather flat shape ($Q = 5.0$ and 10.8 MeV) to a highly anisotropic distribution ($Q = 40.6$ MeV), as compared with phase space (dashed line). The uneven width of the bins chosen for the analysis is due to the limited statistics of the experiment and does not reveal any deficiency in the detection system. For a description of the dotted lines, see text.

very close to threshold, significant contributions of higher partial waves have been reported [9]. Besides showing the deviation from s-wave production for the $Q = 19.9$ and 40.6 MeV measurements, Fig. 5 also presents the prediction of two-step model calculations from Stenmark [31]. The latter were performed to describe the WASA/PROMICE data [13] (Fig. 6), while the predictions in Fig. 5 were evaluated at the corresponding COSY-11 excess energies [32]. The result is in reasonable agreement with the COSY-11 data at $Q =$ 19.9 MeV. However, at $Q = 40.6$ MeV, the shape of the angular distribution in the backward hemisphere does not agree as well. Such a deviation shows up also in the WASA/PROMICE measurements at $Q = 41.1$ MeV [Fig. 6 (b)]. Furthermore, the results from COSY-11 at excess energies of $Q =$

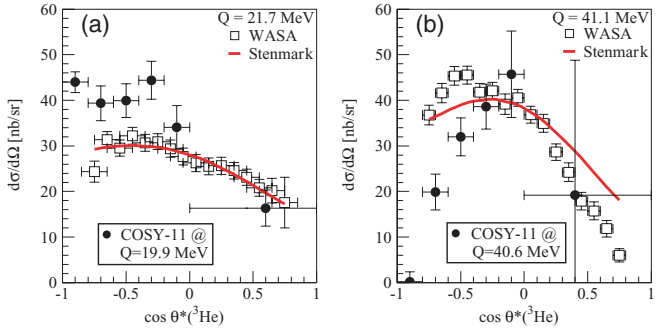

FIG. 6. (Color online) Acceptance-corrected differential cross sections in $\cos\theta^{*}(^{3}\mathrm{He})$ at the two lowest beam energies of Ref. [13]. Dashed line is the calculation by Stenmark based on a two-step model [31]. Solid circles are the present COSY-11 measurements at nearby, but slightly lower, excess energies, as denoted in the legend.

19.9 MeV and $Q = 40.6$ MeV show a behavior of the differential cross sections similar to that of the WASA/PROMICE data. However, the data sets differ significantly in the backward hemisphere (Fig. 6). To clarify this situation, precision data on this topic would be desirable. Currently, new data from ANKE [33] are under evaluation and these might cast light on this discrepancy.

Utilizing the determination of the integrated luminosity via pd elastic scattering [22], the total cross section was extracted for each of the measured excess energies and shown in Fig. 7 and Table II. The normalization uncertainty σ_{norm} is principally due to the luminosity determination from the $pd \to pd$ reaction. The systematic error from the extraction of the η signal from background is only of minor relevance in this respect and only becomes significant at $Q = 40$ MeV, where the statistics are low. The error bars presented, e.g., in Fig. 7 represent the total error as a sum of the systematic, statistical, and normalization errors given in Table II.

Eliminating the phase space factor from the data, the absolute square of the production amplitudes $|f|^2$ is obtained from the differential cross section data using

$$|f|^2 = \frac{p_p^*}{p_\eta^*} \times \frac{\mathrm{d}\sigma}{\mathrm{d}\Omega}, \tag{1}$$

where p_p^* and p_η^* are the momenta of the initial proton and final state η meson in the c.m.s., respectively. This allows an alternative presentation of the data which stresses the

TABLE II. Extracted values for the production amplitude squared and the total cross section for the $pd \to {}^{3}\mathrm{He}\eta$ reaction. The uncertainty in the beam momentum p_{beam} is of the order of 0.1%.

p_{beam} (GeV/c)	Q (MeV)	E_{kin} (MeV)	p_η^* (fm^{-1})	Production amplitude $\lvert f\rvert^2$				Total cross section σ_{tot}			
				(nb/sr)	σ_{stat}	σ_{syst}	σ_{norm}	(nb)	σ_{stat}	σ_{syst}	σ_{norm}
1.581	5.0	900	0.35	592	±12	±38	±64	574	±12	±37	±62
1.593	10.8	911	0.51	327	±10	±41	±34	462	±14	±58	±47
1.602	15.1	918	0.60	227	±12	±22	±24	378	±20	±37	±40
1.612	19.9	927	0.69	187	±14	±16	±19	356	±27	±30	±37
1.655	40.6	964	0.99	109	$^{+71}_{-45}$	$^{+49}_{-45}$	±11	292	$^{+191}_{-121}$	$^{+132}_{-121}$	±30

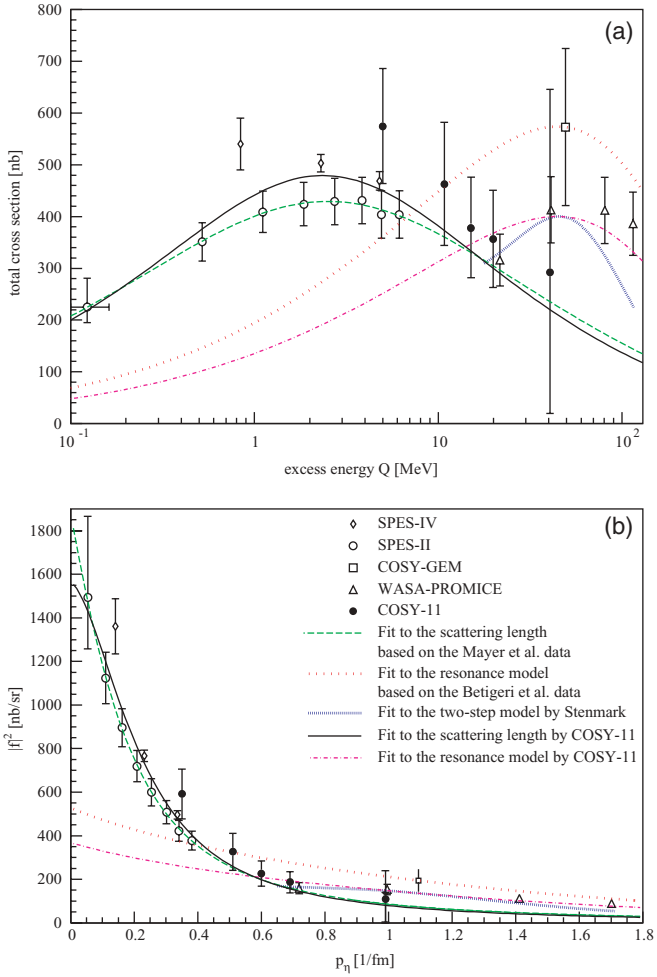

FIG. 7. (Color online) Excitation function of the $pd \to {}^3\mathrm{He}\eta$ production. (a) Total cross section as a function of the excess energy Q. (b) Squared production amplitude as a function of the η c.m.s. momentum. The uncertainty in the η-momentum/excess energy is of the order of the symbol size [34]. The lines represent fits to the data based on the two proposed reaction models: The fit to the Mayer *et al.* data was taken from Ref. [8], the fit to the Betigeri *et al.* data was taken from Ref. [12], and the estimation within the two-step model by Stenmark was taken from Ref. [31].

underlying special features of the reaction process (Fig. 7 and Table II).

Our values of the production amplitudes close the gap between the SATURNE data [7,8] at low energies and the higher energy data from WASA/PROMICE [13] and COSY-GEM [12] (Fig. 7), confirming the strong decrease of the production amplitude from threshold with increasing excess energies.

Fits to the data based on the two proposed reaction models to describe the energy dependence are also presented in Fig. 7. The dotted line with wide gaps represents a Breit-Wigner fit to a purely resonant production mechanism, as proposed by Betigeri *et al.* [12]. Scaling this for an optimized description of all data, including the present COSY-11 measurements above 15 MeV excess energy, yields the dash-dotted line of Fig. 7. Especially in the total cross section plot of Fig. 7, it is obvious that this approach is able to describe the high-energy data, but fails completely to reproduce the shape of the excitation function below $Q = 20$ MeV. Furthermore, the angular distributions presented here, as well as in Refs. [12] and [13], show that at excess energies above 10–20 MeV one cannot assume pure s-wave scattering, and therefore the predominant contribution of an S_{11} resonance is highly unlikely.

The dashed line corresponds to the application of an η-^{3}He FSI ansatz [Eq. (2)] to the data from SATURNE [8], as proposed by Wilkin [6], to refine the energy dependence of the two-step model of Kilian and Nann:

$$|f|^2 = \left|\frac{f_B}{1 - ip_\eta a}\right|^2 = \frac{f_B^2}{1 + 2p_\eta \Im(a) + p_\eta^2 \Im(a)^2 + p_\eta^2 \Re(a)^2}.$$

As well as neglecting the effective range contribution, the implicit assumption here is that f_B varies only slowly with energy.

Although this approach is only valid in the near-threshold region, for demonstration purposes the curve has been extended up to higher excess energies. In addition to the data from Ref. [8], this curve also describes our highest energy data points within the error bars and the lowest energy WASA/PROMICE data point, but fails to describe the data from WASA/PROMICE and COSY-GEM at higher excess energies. However, as already pointed out in Ref. [35], the χ^2/n_{df} of such a fit to the results of Ref. [8] alone is inconsistent with the quoted statistical uncertainties of the data.

A different calculation by Stenmark [31], also exploiting a two-step model approach, is included in Fig. 7 as a dotted line with narrow gaps. This prediction is only valid for higher excess energy data ($Q > 18$ MeV), where higher partial waves contribute to the reaction process. According to Ref. [31], when including FSI effects and assuming that the FSI affects p and d waves by the same amount as it affects s waves, this model is able to roughly reproduce the energy dependence of the WASA/PROMICE data but overestimates the differential cross section.

With the additional data from COSY-11, a fit based on the η-^{3}He scattering length approach has been performed (Fig. 7, solid line). In this fit, only the present results up to an excess energy of 10.8 MeV ($p_\eta = 0.51\ \mathrm{fm}^{-1}$) and the data from Refs. [7,8] have been included, as the FSI calculation from Ref. [6] is only valid for pure s waves and the angular distributions of data above $Q = 10.8$ MeV reveal contributions of higher partial waves, as is obvious in Fig. 5. Based on this data selection, the scattering length a was determined to be $|\Re(a)| = 4.2 \pm 0.5$ fm, $\Im(a) = 0.4 \pm 1.9$ fm, and $f_B = 39.6 \pm 7.6$ nb/sr (Fig. 7, solid line).

Despite the good description of the shape, the curve does not fit perfectly the SPES-II/IV or the COSY-11 data because of a discrepancy in the absolute scale of the extracted total cross sections. Nevertheless, the observed shape of the COSY-11 data strongly supports the predictions for a very strong final state effect.

In Fig. 8, the results of the fitting procedure are presented in a topological view, showing the direct correlation of the real and imaginary parts and the restriction on the absolute value of the real part in the extraction of the scattering length

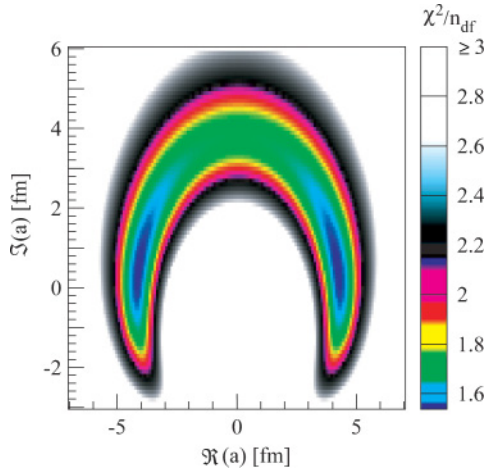

FIG. 8. (Color online) Fit of the scattering length formula in the η-^{3}He FSI model approach to all available data from threshold up to the COSY-11 10.8 MeV measurement. While the real and imaginary parts are binned in 0.1 fm intervals, the amplitude f_B is fitted, and the corresponding χ^2/n_{df} is plotted on the z axis. For a better visualization the range of the z axis is limited to values below 3. The inner dark (blue) areas correspond to the best χ^2 values.

(Eq. (2)). Presented is the χ^2/n_{df} (z axis) for the fit to the data, as a function of the $\Re(a)/\Im(a)$ combinations within the selected range ($\chi^2/n_{df} < 3$).

This presentation allows direct insight into the uncertainty of the fit to the data. In Ref. [35] the η-^{3}He scattering length was extracted in a similar way using only the data from Refs. [7,8], yielding $\Re(a) = 4.3 \pm 0.3$ fm and $\Im(a) = 0.5. \pm 0.5$ fm. Within the uncertainty of the fitting procedures, these values agree with the scattering length we extracted from the extended database that included the COSY-11 results.

Another hint that the observed excitation function is determined in large part by a FSI effect can be obtained by comparing the results presented in Fig. 7 with photoproduction data for $\gamma^3\text{He} \rightarrow {}^3\text{He}\eta$ (Fig. 9). Such measurements have been

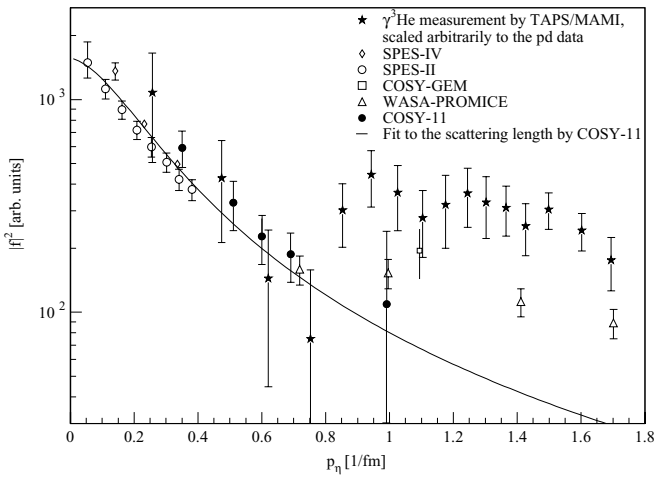

FIG. 9. Squared absolute production amplitude for the η-^{3}He final state in γ^3He and pd collision. The photoproduction data (stars) have been scaled arbitrarily to fit the pd data at $p_\eta < 0.8$ fm^{-1}.

carried out [36], investigating the excitation function from a few MeV above threshold up to the highest WASA/PROMICE excess energy. When scaled arbitrarily to fit the lower energy points to the scattering-length-fit curve to the proton-deuteron data, the shape of the excitation function is consistent with the close-to-threshold data and with the η-^{3}He FSI description.

The photoproduction data [36] reveal an enhancement in the excitation function, as indicated at a lower level by the WASA/PROMICE data [13]. However, when moving to higher excess energies ($p_\eta > 0.8$ fm^{-1}), the different underlying production processes also have to be taken into account. This enhancement might be taken as an indication for an η bound to a ^{3}He, where the real part of the scattering length would have to become relatively large and negative to allow such a state [37]. However, the sign of the real part of the scattering length is not directly accessible, and the experimental data are not sufficient to draw final conclusions from the γ^3He measurements alone. The limited statistics in Ref. [36] leave an ambiguity in the results that makes them compatible with zero [38] and therefore does not allow the differentiation between a bound or a virtually bound state [39]. Even when combining all the available data from different reaction processes that produce the η, as has been done in Ref. [36], there are still no constraints in the interpretation of the data that allow the extraction of the sign of $\Re(a)$.

V. CONCLUSION AND OUTLOOK

The new data from COSY-11 clearly support a strong effect of the η-^{3}He FSI and confirm a strong decrease of the production amplitude $|f|^2$ with increasing excess energy in the region below 20 MeV. Furthermore, an overall fit to the available data below 11 MeV excess energy allows one to extract information on the real and imaginary parts of the scattering length. However, the data, especially in the near-threshold region, are not sufficient to determine with precision both the real and imaginary parts. This leads to the conclusion that the extraction of the η-^{3}He scattering length with high accuracy from the excitation function requires very precise near-threshold data from a single experimental facility. Such additional measurements have in fact been performed recently [33,40].

Furthermore, it is seen that up to now, none of the theoretical models can describe the excitation function over the whole range of measured beam momenta. A two-step model approach, such as that in Ref. [31] for higher excess energies, when combined with a final state refinement [6] to account for the special energy dependence in the near-threshold region is a promising candidate for a comprehensive description of the excitation function. Further theoretical and experimental work in this field will be of great value.

ACKNOWLEDGMENTS

The authors thank the COSY crew for providing such an excellent beam for the experiment, and C. Wilkin, M. Stenmark, and C. Hanhart for their contributions,

fruitful discussions, and support during the preparation of this paper. We acknowledge the support of the European Community Access to Research Infrastructure Action of the Improving Human Potential Programme (Hadron Physics, Contract No. RII3-CT-2004-506078), the Research Centre Jülich (FFE Grant Nos. 41266606 and 41266654), the DAAD Exchange Program (PPP-Polen), the Polish State Committee for Scientific Research (Grant No. PB1060/P03/2004/26), and the RII3/CT/2004/506078, Hadron Physics Activity, N4:EtaMesonNet.

[1] Q. Haider and L. Liu, Phys. Lett. **B172**, 257 (1986).
[2] R. S. Bhalerao and L. C. Liu, Phys. Rev. Lett. **54**, 865 (1985).
[3] A. M. Green and S. Wycech, Phys. Rev. C **71**, 014001 (2005).
[4] P. Moskal *et al*., Phys. Rev. C **69**, 025203 (2004).
[5] S. D. Bass and A. Thomas, Phys. Lett. **B634**, 368 (2006).
[6] C. Wilkin, Phys. Rev. C **47**, R938 (1993).
[7] J. Berger *et al*., Phys. Rev. Lett. **61**, 919 (1988).
[8] B. Mayer *et al*., Phys. Rev. C **53**, 2068 (1996).
[9] V. Nikulin *et al*., Phys. Rev. C **54**, 1732 (1996).
[10] K. Kilian and H. Nann, AIP Conf. Proc. **221**, 185 (1990).
[11] G. Fäldt and C. Wilkin, Phys. Lett. **B354**, 20 (1995).
[12] M. Betigeri *et al*., Phys. Lett. **B472**, 267 (2000).
[13] R. Bilger *et al*., Phys. Rev. C **65**, 44608 (2002).
[14] R. Maier, Nucl. Instrum. Methods A **390**, 1 (1997).
[15] S. Brauksiepe *et al*., Nucl. Instrum. Methods A **376**, 397 (1996).
[16] P. Moskal *et al*., Nucl. Instrum. Methods A **466**, 448 (2001).
[17] J. Smyrski *et al*., Nucl. Instrum. Methods A **541**, 574 (2005).
[18] H. Dombrowski *et al*., Nucl. Instrum. Methods A **386**, 228 (1997).
[19] M. Rook, Dissertation, Universität Bonn, Berichte des FZ Jülich; Jül-2922, 1994; ISSN 0944-2952.
[20] M. Rook, Diploma thesis, Universität Köln, Berichte des FZ Jülich; Jül-2407, 1990; ISSN 0366-0885.
[21] COSY-11 Collaboration, Annual Report, IKP FZ Jülich, 1996 (unpublished), p. 38.
[22] H.-H. Adam, Dissertation, Universität Münster (in preparation).
[23] The value of the ^{3}He nucleus mass used in the calculations for the described analysis is $m_{^3\mathrm{He}} = 2.808392\ \mathrm{GeV}/c^2$.
[24] H.-H. Adam, Diploma thesis, Universität Münster, 2000.
[25] GEANT-detector description and simulation tool, CERN Program Library Long Writeup W5013, CERN, 1211 Geneva 23, Switzerland.
[26] P. Moskal *et al*., J. Phys. G **32**, 629 (2006).
[27] E. Gülmez *et al*., Phys. Rev. C **43**, 2067 (1991).
[28] E. Coleman *et al*., Phys. Rev. **164**, 1655 (1967).
[29] N. Booth *et al*., Phys. Rev. D **4**, 1261 (1971).
[30] E. Winkelmann, P. R. Bevington, M. W. McNaughton, H. B. Willard, F. H. Cverna, E. P. Chamberlin, and N. S. P. King, Phys. Rev. C **21**, 2535 (1980).
[31] M. Stenmark, Phys. Rev. C **67**, 034906 (2003).
[32] M. Stenmark (private communication), 2005.
[33] A. Khoukaz *et al*., COSY Proposal No. 137, 2004 (unpublished).
[34] P. Moskal *et al*., Phys. Lett. **B474**, 416 (2000).
[35] A. Sibirtsev *et al*., Eur. Phys. J. A **22**, 495 (2004).
[36] M. Pfeiffer *et al*., Phys. Rev. Lett. **92**, 252001 (2004).
[37] V. Baru, J. Haidenbauer, C. Hanhart, and J. A. Niskanen, Phys. Rev. C **68**, 035203 (2003).
[38] A. Sibirtsev, J. Haidenbauer, J. A. Niskanen, and Ulf-G. Meißner, Phys. Rev. C **70**, 047001 (2004).
[39] C. Hanhart, Phys. Rev. Lett. **94**, 049101 (2005).
[40] J. Smyrski *et al*., COSY Proposal No. 142, 2004 (unpublished).